

Scalable Synthesis of CoMn_2O_4 Nanorods and their Operating-Temperature-Dependent Li-Ion Storage Behaviour

Zhen-Dong Huang*, Ting-Ting Zhang, Hao Lu, Yanwu Fang, Ling Bai, Rui-Qing Liu, Xiu-Jing Lin, Pan Li, Yi Li, Xiaomiao Feng, Yanwen Ma*

Key Laboratory for Organic Electronics and Information Displays & Institute of Advanced Materials (IAM), National Synergistic Innovation Center for Advanced Materials (SICAM), Nanjing University of Posts & Telecommunications, 9 Wenyuan Road, Nanjing, China

*Corresponding Author: Zhen-Dong Huang, Key Laboratory for Organic Electronics and Information Displays & Institute of Advanced Materials (IAM), National Synergistic Innovation Center for Advanced Materials (SICAM), Nanjing University of Posts & Telecommunications, 9 Wenyuan Road, Nanjing, China

Received Date: 08-07-2017

Accepted Date: 28-07-2017

Published Date: 05-08-2017

ABSTRACT

Binary transition metal oxides have attracted increasing attention as potential anode materials for next generation lithium ion batteries. Herein, the highly temperature dependent Li-ion storage behaviours of as-produced CoMn_2O_4 nanorods are characterized by using cyclic voltammetry and galvanostatic charge/discharge at a wide range of operating temperature. The CoMn_2O_4 nanorod shows relatively higher capacity and better cyclic stability under the temperature ranged from 10 to 40 °C. Effective solutions are required to further optimize its low-temperature electrochemical activity and high-temperature cyclic stability in the future work so as to satisfy the all-weather application.

Keywords: Lithium ion batteries; Anode materials; Transition metal oxides, Temperature dependant Li-ion storage behaviour; Rheological phase method

INTRODUCTION

From the end of the 20th century, lithium ion batteries (LIBs) have been employed as the dominant power sources for various portable electronic devices, and one of the most promising battery system for large-scale applications in hybrid and plug-in hybrid electric vehicles, solar and wind electricity generation systems, due to the advantages such as high energy density, good cyclic stability and environmental benignity.^{1, 2} In order to meet the ever-increasing requirements to LIBs from the market multi-applications, various nanostructured transitional metal oxides, especially Mn_3O_4 , Co_3O_4 and its derivatives, have been developed as novel anodes over the past decade.¹⁻³ Amongst the available materials, $\text{Co}_x\text{Mn}_{3-x}\text{O}_4$ mixed oxides have attracted increasing attention as potential anode materials for next generation LIBs, owing to the synergistic natures such as higher conductivity, larger reversible capacity, and better mechanical stability.⁴

Major attention have been paid on developing a wide variety of synthetic approaches towards

$\text{Co}_x\text{Mn}_{3-x}\text{O}_4$ nanostructures, such as hierarchical CoMn_2O_4 array,⁴ microsphere,⁵ hollow microcubes,⁶ nanorod.⁷ There into, the 1D nanorod morphology not only has a large specific surface area but also provides efficient charge transport pathways and facile strain relaxation during battery charge and discharge.⁸ For example, a single-crystalline CoMn_2O_4 nano/ submicrorods prepared by using a low-cost and facile approach by using $\beta\text{-MnO}_2$ nanorods as both the template and manganese source material demonstrate good electrochemical performance with a high reversible capacity of 520 mAh g^{-1} at a current density of 200 mA g^{-1} after 100 cycles.⁷

It is a very common sense that nanoscale active materials normally exhibit better electrochemical performance than that of their (sub)-microscale counterparts, while it is still important to understand the detailed influences of the particle size and morphology on the final electrochemical performance of active materials.^{9, 10} Analogously, it is also vital to find out the effect of the operating

Scalable Synthesis of CoMn_2O_4 Nanorods and their Operating-Temperature-Dependent Li-Ion Storage Behaviour

temperature on the electrochemical performance of different electrode materials. Because LIBs have to work in a wide range of the realistic operating temperature from ~ -20 to 55°C for all-weather daily application in different seasons or locations.^{11, 12}

Thus, many works have been done to understand the concrete effects of the operating temperature on the electrochemical performance of different electrode materials, such as LiFePO_4 ,¹³ $\text{Li}[\text{Co}_{0.1}\text{Ni}_{0.15}\text{Li}_{0.2}\text{Mn}_{0.55}]\text{O}_2$,¹⁴ even though it is also well known that batteries function more properly at room temperature, any deviation towards hot and cold changes the performance and/or calendar life. Moreover, to the best of our knowledge, few reports focus on the lithium ion storage performance of CoMn_2O_4 at both low and high temperatures. Based on the above considerations, we try to fabricate the controllable CoMn_2O_4 nanorods by a template-assisted rheological phase method modified by a

temperature reduction annealing process. The operating-temperature-dependent Li-ion storage behavior of CoMn_2O_4 nanorods is also detailedly studied in this work.

EXPERIMENTAL

Preparation of $\beta\text{-MnO}_2$ Nanorods

$\beta\text{-MnO}_2$ nanorods were synthesized by a hydrothermal method.⁸ In a typical synthesis process, $\text{Mn}(\text{C}_2\text{H}_3\text{O}_2)_2 \cdot 4\text{H}_2\text{O}$ and $\text{Na}_2\text{S}_2\text{O}_8$ were dissolved in 80 mL of distilled water by magnetic stirring to form a clear solution at room temperature with a molar ratio of 1:1. Successively, the mixed solution was transferred to a 100 mL Teflon-lined stainless steel autoclave and heated at 120°C for 12 h in a preheated electric oven for the hydrothermal reaction. After being washed with water and ethanol for three times, respectively, $\beta\text{-MnO}_2$ nanorods were dried at 80°C for 10 h and collected for the preparation of CoMn_2O_4 nanorods.

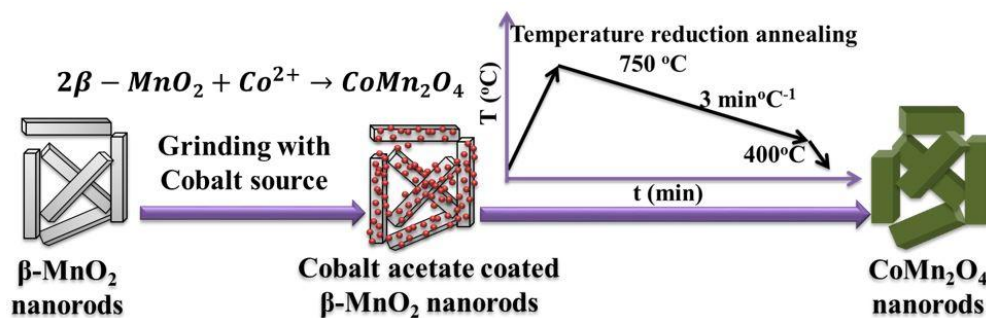


Figure 1. Schematic illustration of the synthesis processes for CoMn_2O_4 nanorods.

Controllable Preparation of CoMn_2O_4 Nanorods

A modified template-assisted rheological phase method is employed to prepare CoMn_2O_4 nanorods. Fig. 1. schematically illustrates the typical synthesis process. The as-prepared $\beta\text{-MnO}_2$ nanorods were used as template and manganese source. Subsequently, 0.002 moles of $\text{Co}(\text{C}_2\text{H}_3\text{O}_2)_2 \cdot 4\text{H}_2\text{O}$, and 0.004 moles of the as-synthesized $\beta\text{-MnO}_2$ were dispersed into 5 mL high purity ethanol to form a thick slurry, ground to form a fine mixture for 30 mins, and dried at room temperature. The above process was repeated three times to produce a well-mixed powder. The powder was then calcined in a muffle furnace.

A stepwise temperature-reduction crystallization process is applied to optimize the morphology and crystallinity of final CoMn_2O_4 nanorod product. The furnace was first heated to 750°C at the rate of $10^\circ\text{C min}^{-1}$ in air, and then slowly cooled to 400°C in a speed of 3 min^{-1} . After a furnace cooling process, the as-prepared CoMn_2O_4 nanorods were finally obtained.

Characterization

The morphologies of $\beta\text{-MnO}_2$ and CoMn_2O_4 were characterized by using scanning electron microscopy (Hitachi S-4800) at an acceleration voltage of 15 kV. The crystal structure of the as-prepared $\beta\text{-MnO}_2$ and CoMn_2O_4 were measured on an X-ray diffractometer (RIGAKU, RINT-ULTIMA III) using Cu K α radiation ($\lambda = 1.54051\text{\AA}$). The diffraction patterns were recorded in the 2θ range of $10\text{-}70^\circ$ with a step size of 0.01° . The Scherrer equation, namely $D = K\lambda/\beta\cos\theta$, was used to estimate the average grain size. In order to investigate the electrochemical performance of as-prepared CoMn_2O_4 nanorod, the composite electrodes of CoMn_2O_4 were prepared by coating the uniform slurry of CoMn_2O_4 mixed with acetylene black (AB) and Polyvinylidene fluoride (PVDF) ($\text{CoMn}_2\text{O}_4/\text{C}/\text{PVDF} = 80/15/5$). The electrode was then pressed and punched out into 10 mm disks in diameter. Two-electrode lithium ion batteries were assembled in an ultrapure Ar-gas filled glove box to study the lithium ion storage performance of CoMn_2O_4 in 1 mol L^{-1} LiClO_4

Scalable Synthesis of CoMn_2O_4 Nanorods and their Operating-Temperature-Dependent Li-Ion Storage Behaviour

electrolyte. Lithium discs were used as counter and reference electrodes. Cyclic voltammetry (CV) and galvanostatic charge and discharge

measurements were carried out in the electrolytic window range of 0.01 to 3 V vs Li/Li^+ at -20 to 55 °C at 0.5 mV s^{-1} and 460 mA g^{-1} , respectively.

RESULTS AND DISCUSSION

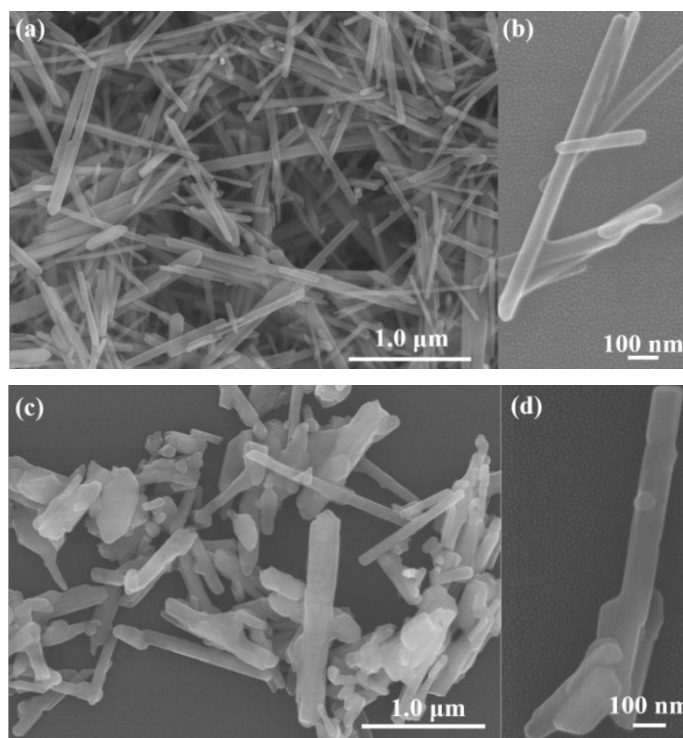


Figure 2. Scanning electron microscopy (SEM) images of as-prepared $\beta\text{-MnO}_2$ (a, b) and CoMn_2O_4 (c, d) nanorods.

Morphology

Fig. 2 shows morphologies of as-prepared $\beta\text{-MnO}_2$ and CoMn_2O_4 . As shown in Fig. 2a, uniform nanorods can be obviously observed. The high resolution SEM image shown in Fig. 2b further indicates that the length and the diameter of as-prepared MnO_2 nanorods are $\sim 2 \mu\text{m}$ and $\sim 50 \text{nm}$, respectively. Being uniformly mixed, a temperature-reduction annealing process (see Fig. 1) was applied to crystallize the mixture of MnO_2 template and $\text{Co}(\text{C}_2\text{H}_3\text{O}_2)_2 \cdot 4\text{H}_2\text{O}$, meanwhile to avoid the great increase of

particle size and to maintain the nanorod feature.^{15, 16} As expected, the final CoMn_2O_4 product maintain the nanorod shape of MnO_2 , see the SEM images in Fig. 2c and 2d. With the introduction of Co^{3+} component and the merges of two and more rods together during calcination process, the diameter of obtained CoMn_2O_4 increase to 100 nm. However, comparing to $\beta\text{-MnO}_2$ nanorods, the length decrease to $\sim 1 \mu\text{m}$. Shortening of rod length might be caused by the uneven inner stress generated during the formation and growth of the CoMn_2O_4 from MnO_2 .

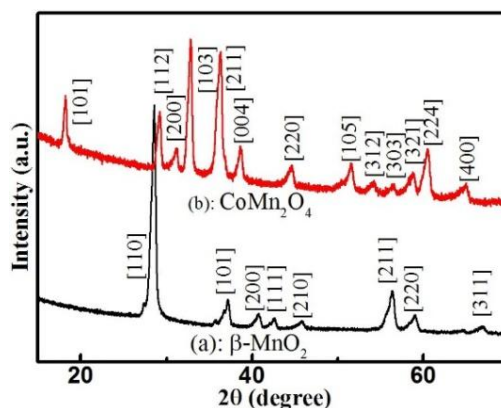


Figure 3. X-ray diffraction patterns of as-prepared $\beta\text{-MnO}_2$ (a) and CoMn_2O_4 nanorods (b)

Crystal Structure

Fig. 3 presents the crystal structure of as-prepared $\beta\text{-MnO}_2$ and CoMn_2O_4 . The XRD pattern shown in Fig. 3a is properly indexed as $\beta\text{-MnO}_2$ without obvious diffraction peaks of any impurity.

⁸While the XRD pattern shown in Fig. 3b could be indexed as body-centered tetragonal (bct) phase. No diffraction peaks of precursor and other impurity phase can be found.⁵⁻⁷ Based on Scherrer equation, an average grain size of ~ 17 nm is estimated from peak (103).

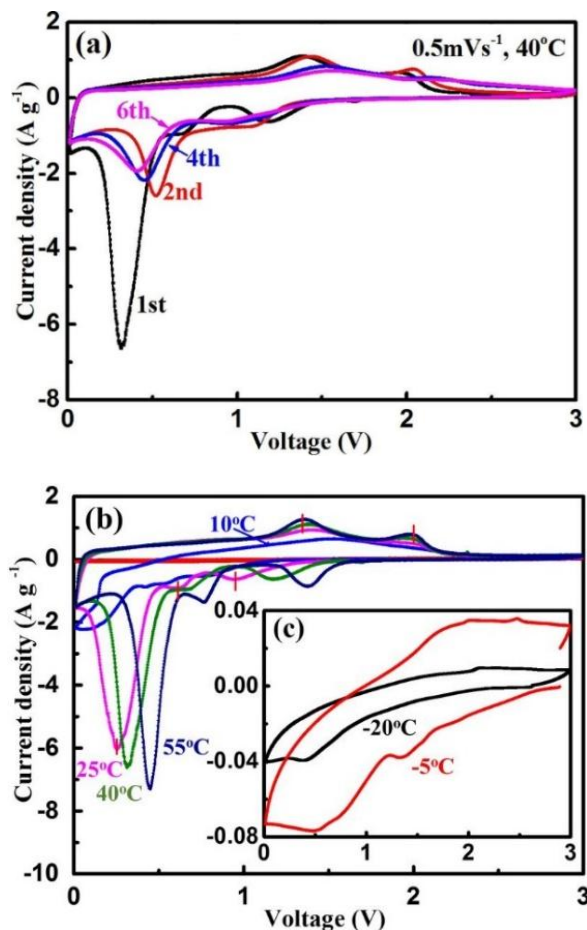


Figure 4. Cyclic voltammetry curves of CoMn_2O_4 nanorod composite electrodes: (a) initial 6 CV cycles scanning at 0.5 mV s^{-1} under 40°C , (b) and inset (c) 1st cycle CV curves obtained at 0.5 mV s^{-1} under different temperatures.

Cyclic voltammetry

Fig. 4 shows the CV curves of the CoMn_2O_4 nanorod composite electrodes at a scan rate of 0.5 mV s^{-1} over the range of $0.01\text{--}3.00 \text{ V}$. Fig. 4a demonstrates the first six consecutive CV curves of the electrode made by CoMn_2O_4 nanorods under 40°C . Three reduction peaks can be found in the cathodic polarization process of the 1st cycle CV curve, which is different from those of the subsequent ones. This observation is similar with most of the reported results.

The broad peak centered at 1.18 V is ascribed to the reduction of Mn^{3+} to Mn^{2+} ; the intense peak located at 0.32 V could be assigned to the further reduction of Mn^{2+} and Co^{2+} to metallic Mn and Co, respectively; while the minor peak at 0.67 V can be ascribed to the irreversible decomposition

of the solvent in the electrolyte to form the solid-electrolyte interface (SEI).^{5,7} Additionally, there are two oxidation peaks in the following anodic sweep; the one at 1.38 V is due to the oxidation of Mn to Mn^{2+} , while the other peaks at 1.98 V is caused by the oxidation of Co to Co^{2+} . Started from the 2nd cycle onwards, only two pairs of distinct redox peaks, namely $0.53/1.47 \text{ V}$ and $1.05/2.04 \text{ V}$, can be found in the CV curves, which are corresponding to the reduction/oxidation of MnO and CoO, respectively. Meanwhile, the voltage gaps of both redox pairs slight increase with the formation of irreversible SEI. Fig. 4b and inset 4c demonstrate the CV curves measured at the temperature ranged from -20 to 55°C . It can be found when the operating temperature decreases from 55 to -20°C , the

Scalable Synthesis of CoMn_2O_4 Nanorods and their Operating-Temperature-Dependent Li-Ion Storage Behaviour

reduction peaks shift toward lower voltage while the oxidation peaks move to higher voltage with decreasing peak currents. This observation indicates that the Li-ion storage performance of CoMn_2O_4 nanorods highly depends on the operating temperature. Especially when the

operating temperature is lower than $\sim 10^\circ\text{C}$, the intense peak assigned to the further reduction of Mn^{2+} and Co^{2+} to metallic Mn and Co, respectively, gradually disappear due to the large polarization resulted from the dramatically increased inner and contact resistances.

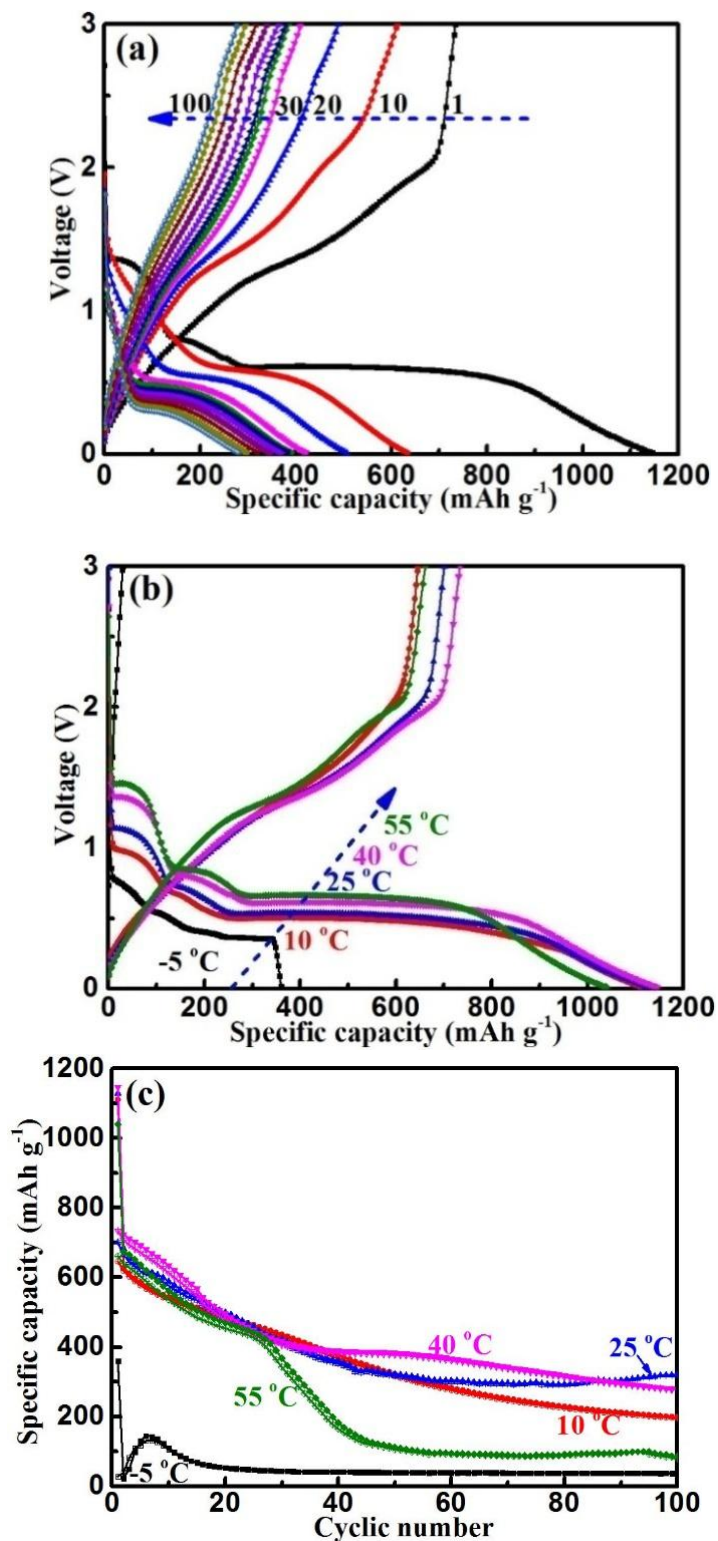


Figure 5. Galvanostatic charge and discharge performance of CoMn_2O_4 nanorod composite electrodes at 460 mA g⁻¹: (a) voltage-capacity profiles from 1 to 100 cycles under 40 oC, (b) the 1st cycle voltage-capacity profiles and (c) long term cyclic performance under different operating temperature.

Galvanostatic Charge/ Discharge Measurements

Fig. 5 presents the Li-ion storage performance obtained from the galvanostatic charge/discharge measurements. As shown in Fig. 5a, the charge/discharge specific capacity of as-produced CoMn_2O_4 nanorod are 1145 and 733.8 mAh g^{-1} at the current density of 460 mA g^{-1} under operating condition of 40 °C, respectively. The initial charge capacity is higher than the theoretical value of 920 mAh g^{-1} based on the conversion reaction: $\text{CoMn}_2\text{O}_4 + 8\text{Li}^+ + 8\text{e}^- \rightarrow \text{Mn} + \text{Co} + 4\text{Li}_2\text{O}$.

The excess capacities could be associated with the decomposition of the electrolyte at low voltages generating a SEI layer and the further lithium storage via interfacial charging at the metal/ Li_2O interface.⁵ The incomplete decomposition of the formed SEI film during the first discharge might be accounted for the large irreversible capacity loss of the first cycle. Interestingly, the discharge specific capacity is also higher than the theoretical capacity of 691 mAh g^{-1} based on the reaction: $3\text{Li}_2\text{O} + \text{Co} + 2\text{Mn} \rightarrow 2\text{MnO} + \text{CoO} + 6\text{Li}^+ + 6\text{e}^-$.⁷ The additional capacity could be derived from the further oxidation of Co^{2+} and Mn^{2+} to Co^{3+} and Mn^{3+} , respectively, as well as the release of interfacial Li^+ and the partial dissolution of the formed SEI. Similar with the reported CoMn_2O_4 and other similar metal oxide,⁴⁻⁷ the as-synthesized CoMn_2O_4 nanorod exhibits a reasonable and comparable cyclic performance. The discharge capacity retain 277 mAh g^{-1} after 100 cycles. The capacity loss during the subsequent cycles should be attributed to the decreased utilization of active materials and the increase of the SEI thickness, see the gradually shorter charge/discharge plateaus and the larger voltage gap in Fig. 5a. Different solution, such as design of the hierarchical nanostructure and control of composition, have been developed to improve the cyclic stability of transition metal and its oxides. Fig. 5b shows the charge/discharge profiles of CoMn_2O_4 nanorod tested at 460 mAh g^{-1} under five different temperatures. The observed results again evidently indicate that the Li-ion storage properties of CoMn_2O_4 highly depend on the operating temperature. The charge plateaus voltage and specific capacity obviously decrease with the decrease of the operating temperature from 55 to -5 °C. Especially when the operating temperature is as lower as -5 °C, CoMn_2O_4 start to lose its Li-ion storage capability. This phenomenon is consistent with the observed CV results shown in

Fig. 4b. Inversely, the cyclic stability become worse when the temperature reach 55 °C, see Fig. 5c. The capacity retention ratio cycled under -5, 10, 25, 40 and 55 °C for 100 cycles at the current density of 460 mAh g^{-1} are 126.9%, 30.3%, 45.7%, 37.8% and 12.1%, respectively. Generally, the CoMn_2O_4 nanorod shows relatively higher capacity and better cyclic stability under the temperature ranged from 10 to 40 °C. Thus, approaches to effectively improve the low temperature electrochemical properties and high temperature cyclic stability will be developed in future studies.

CONCLUSIONS

The CoMn_2O_4 nanorods (100 nm in diameter and $\sim 1\mu\text{m}$ in length) were successfully synthesized by template-assisted rheological phase method modified with a temperature reduction annealing process. The highly temperature dependent Li-ion storage behavior of as-produced CoMn_2O_4 nanorods have been studied in detail by using cyclic voltammetry and galvanostatic charge/discharge.

The discharge specific capacity of as-produced CoMn_2O_4 nanorods are 661.0, 733.8, 700.7, 646.0, and 29.17 mAh g^{-1} at the current density of 460 mA g^{-1} under operating condition of 55, 40, 25, 10, and -5 °C, respectively. After 100 cycles, the capacity retention ratio are 126.9%, 30.3%, 45.7%, 37.8% and 12.1%, respectively. Generally, the CoMn_2O_4 nanorod shows relatively higher capacity and better cyclic stability under the temperature ranged from 10 to 40 °C.

Proper approaches are going to be further investigated to effectively improve the low temperature electrochemical properties by reducing the huge charge transfer and contact resistance and high temperature cyclic stability by enhancing the thermal and structural stabilities of CoMn_2O_4 in the future studies.

ACKNOWLEDGMENTS

This work was supported by National Natural Science Foundation of China (51402155), Priority Academic Program Development of Jiangsu Higher Education Institutions (PAPD) (YX03001), National Synergistic Innovation Center for Advanced Materials (SICAM), and Scientific research foundation of NUPT (NY214021).

REFERENCES

- [1] D.H. Ge, H.B. Geng, J.Q. Wang, J.W. Zheng, Y. Pan, X.Q. Cao, H.W. Gu, *Nanoscale*, 2014, 6, 9689.
- [2] H.L. Wang, L.F. Cui, Y. Yang, H.S. Casalongue, J.T. Robinson, Y. Liang, Y. Cui and H.J. Dai. *J. Am. Chem. Soc.*, 2010, 132, 13978.
- [3] Y.F. Deng, L.N. Wan, Ye. Xie, X.S. Qin, and G.H. Chen, *RSC Adv.*, 2014, 4, 23914.
- [4] L. Yu, L. Zhang, H.B. Wu, G.Q. Zhang and X.W. Lou, *Energy Environ. Sci.*, 2013, 6, 2664.
- [5] L. Hu, H. Zhong, X.R. Zheng, Y.M. Huang, P. Zhang, Q.W. Chen, *Sci. Rep.*, 2012, 2, 986.
- [6] L. Zhou, D.Y. Zhao, X.W. Lou, *Adv. Mater.*, 2012, 24, 745.
- [7] L.J. Wang, B. Liu, S.H. Ran, L.M. Wang, L.N. Gao, F.Y. Qu, D. Chen and G.Z. Shen, *J. Mater. Chem. A*, 2013, 1, 2139.
- [8] D.K. Kim, P. Muralidharan, H.W. Lee, R. Ruffo, Y. Yang, C.K. Chan, H.L. Peng, R.A. Huggins, and Y. Cui, *Nano Lett.*, 2008, 8, 3948.
- [9] Y.C. Chang, C.T. Peng, I.M. Hung, *J. Mater. Sci.*, 2014, 49, 6907.
- [10] N. Wu, Y. X. Yin, Y. G. Guo, *CHEM-ASIAN J.*, 2014, 9, 2099.
- [11] Y. Ji, Y.C. Zhang, C.Y. Wang, *J. Electrochem. Soc.*, 2013, 160, A636.
- [12] A. Yaqub, Y.J. Lee, M.J. Hwang, S.A. Pervez, U. Farooq, J.H. Choi, D. Kim, H.Y. Choi, S.B. Cho, C.H. Doh, *J. Mater. Sci.*, 2014, 49, 7707.
- [13] C.T. Hsieh, C.T. Pai, Y.F. Chen, P.Y. Yu, R.S. Juang, *Electrochimica Acta*, 2014, 115, 96.
- [14] C.H. Yo, J.H. Ju, G.O. Kim, M.J. Hwang, K.S. Ryu., *Ionics*, 2012, 18, 19.
- [15] Z.D. Huang, X.M. Liu, B. Zhang, S.W. Oh, P.C. Ma and J.K. Kim, *Scripta Mater.*, 2011, 64, 122.
- [16] Z.D. Huang, X.M. Liu, S.W. Oh, B. Zhang, P.C. Ma and J.K. Kim, *J. Mater. Chem.*, 2011, 21, 10777.
- [17] J.F. Li, S.L. Xiong, X.W. Li and Y.T. Qian, *Nanoscale*, 2013, 5, 2045.